Dynamics of nanoparticles in solutions of semiflexible ring polymers

Shivraj B. Kotkar,[†] Ryan Poling-Skutvik,[‡] Michael P. Howard,[¶] Arash Nikoubashman,[§,‖] Jacinta C. Conrad,[*,†] and Jeremy C. Palmer[*,†]

[†]*Department of Chemical and Biomolecular Engineering, University of Houston, Houston, TX 77204*

[‡]*Department of Chemical Engineering, University of Rhode Island, Kingston, RI 02881*

[¶]*Department of Chemical Engineering, Auburn University, Auburn, AL 36849*

[§]*Leibniz-Institut für Polymerforschung Dresden e.V., Hohe Straße 6, 01069 Dresden, Germany*

[‖]*Institut für Theoretische Physik, Technische Universität Dresden, 01069 Dresden, Germany*

E-mail: jcconrad@uh.edu; jcpalmer@uh.edu

Abstract

We use hybrid molecular dynamics-multiparticle collision dynamics simulations (MD–MPCD) to investigate the influence of chain stiffness on the transport of nanoparticles (NPs) through solutions of semiflexible ring polymers. The NPs exhibit subdiffusive dynamics on short time scales before transitioning to normal diffusion at longer times. The terminal NP diffusivities decrease with increasing ring stiffness, similar to the behavior observed in solutions of semiflexible linear chains. The NP subdiffusive exponent is found to be strongly correlated with that of the polymer center-of-mass (COM) for the range of chain stiffnesses examined, which is at odds with the pronounced decoupling of the NP and polymer COM motions previously observed upon increasing the stiffness of linear chains. Our analysis indicates that these marked differences in the intermediate dynamics are rooted in distinct structural changes that emerge with increasing bending stiffness: stiffer ring polymers adopt increasingly circular conformations and stack into transient tubes. The void space created near the ring centers is occupied by NPs and other polymers, resulting in a strong dynamic coupling on short time scales.

1 Introduction

The transport of nanoparticles (NPs) through polymer solutions is encountered in applications ranging from hydrocarbon exploration[1] to drug delivery[2–7] to nanocomposite processing.[8–13] Transport through Newtonian fluids is well-described by the Stokes–Einstein relation (SER), which predicts that the NP diffusivity is inversely proportional to the zero-shear solution viscosity. The SER can be generalized to complex fluids by incorporating a frequency-dependent solution viscosity.[14,15] Both the SER and the generalized SER, however, assume that the transported NPs are larger than the characteristic length scales associated with heterogeneities in the background fluid. In complex fluids, this assumption breaks down when the NP size is comparable to the polymer radius of gyration or mesh size, resulting in measured dynamics that are faster than predicted from the solution's zero-shear viscosity.[16–21]

The factors governing NP transport in this size regime have been investigated in several computational[22–29] and theoretical[30–35] studies. Although most of these studies have focused on flexible linear chains, polymers found in many settings often have other architectures and different degrees of flexibility. Circular or ring-like architectures, for example, are commonly used to model chromatin[36–39] and are observed to form in semiflexible biopolymers such as DNA.[40–42] Ring polymers exhibit distinct structural and dynamical properties due to their closed conformations.[36,37,41–50] Examples include the faster relaxation of ring polymers compared to linear chains of the same molecular weight[44] due to the absence of free ends, which allows ring polymers to avoid or delay entanglements.[51] Additionally, inter-ring threadings, or penetrations, can also lead to a topological glass transition in concentrated solutions and melts, which has not been reported to occur for linear chains.[52]

The distinct properties of ring polymers and their effects on NP transport remain incompletely understood. Simulation studies have investigated NP transport in entangled ring polymer systems,[39,53] finding faster NP motions in melts of ring polymers than in similar systems of linear chains due to the absence of long-lived entanglement tubes in the former. The effects of chain flexibility on the NP dynamics have been also compared in polymer melts with linear and circular architectures. NP dynamics were found to be faster in melts of stiff linear chains compared to rings with the same stiffness, but the opposite behavior was observed for flexible systems.[54] Langevin dynamics (LD) simulations have also been performed to investigate the influence of NP size on transport in weakly entangled solutions of ring and linear polymers.[55] NPs were found to diffuse faster in solutions of ring polymers than in solutions of linear polymers when the NP size was larger than the tube diameter. For smaller NPs, however, the diffusivities were found to be comparable in ring and linear polymer solutions, which was posited to be due to the similarity of the Rouse dynamics on these length scales.[55] Finally, increasing the concentration of NPs in ring polymer melts was found to lead to a slowing of the dynamics of the ring polymers; further, the dynamics decreased sharply at high NP concentrations as more monomers come into contact with

multiple NPs.[56]

These prior studies provide insight into how polymer architecture and stiffness influence NP dynamics in concentrated and/or entangled systems. However, much less is known about their effects on NP transport in unentangled (semi)dilute solutions, which is characteristic of many biological systems.[57–59] At such concentrations, long-range hydrodynamic interactions (HI) may also influence the dynamics, necessitating careful modeling of these effects.[60–62] In our recent studies, we used a hybrid molecular dynamics–multiparticle collision dynamics (MD–MPCD) scheme to perform hydrodynamic simulations of NP dynamics in unentangled, semidilute solutions of polymers.[26–28,63] NP dynamics were found to be remarkably insensitive to the polymer architecture when compared in solutions of flexible linear chains and rings with similar monomer concentrations.[28] For both systems, the scaling behavior of the long-time NP diffusivities was well-described by a recently developed polymer coupling theory (PCT),[30] which assumes that NP motions fully couple to the segmental Rouse dynamics of the polymers. The short-time subdiffusive NP dynamics, by contrast, were found to be faster than predicted by PCT. This finding was attributed to the NPs coupling to polymer center-of-mass (COM) motions on short time scales, which is an additional coupling mechanism that is not accounted for by PCT.[28]

Although the architecture of flexible polymers was not found to strongly influence NP dynamics, our previous MD–MPCD study of semiflexible linear chains demonstrated that polymer stiffness has an appreciable effect.[27] As chain stiffness was increased, the long-time NP diffusivities exhibited increasing deviations from PCT, which was developed for fully flexible chains. The short-time subdiffusive NP dynamics also became increasingly decorrelated with the polymer COM motions. These effects were hypothesized to arise from changes in the segmental mobility as the stiffness of the chains increased.

To understand the combined effects of ring-shaped polymer topology and bending stiffness, we have performed a complementary study of NP dynamics in solutions of semiflexible ring polymers using MD–MPCD simulations. Similar to the behavior observed for semiflex-

ible linear chains, the NP diffusivities decrease as polymer stiffness increases. In contrast with the behavior observed for semiflexible linear chains, however, the NP and polymer COM subdiffusive dynamics remain strongly correlated across the range of chain stiffnesses examined. Our analysis indicates that structural changes in the ring polymer solutions allow the NP and polymer COM subdiffusive motions to remain highly coupled even as the segmental motions change upon stiffening.

2 Methods

Hybrid MD–MPCD[62,64,65] simulations of spherical NPs in solutions of semiflexible ring polymers were performed using LAMMPS (ver. 22Aug18).[66] For simplicity, we describe the model parameters of the system using fundamental units σ, m, and ε for length, mass, and energy, respectively. The corresponding unit of time is expressed in these fundamental units as $\tau = \sqrt{m\sigma^2/\varepsilon}$. All model parameters and physical quantities derived from the simulations are reported in these units.

The model is similar to the one used in our prior study of NP dynamics in solutions of flexible ring polymers.[28] The ring polymers consist of N_m monomer beads, each with a diameter of σ_m, whereas the NPs are modeled as single large beads of diameter σ_NP. Excluded volume interactions between particles are modeled with a shifted Weeks–Chandler–Andersen (sWCA)[67] potential:

$$U_\mathrm{sWCA}(r_{ij}) = \begin{cases} 4\varepsilon\left[\left(\dfrac{\sigma_{ij}}{r_{ij}-\Delta_{ij}}\right)^{12} - \left(\dfrac{\sigma_{ij}}{r_{ij}-\Delta_{ij}}\right)^{6}\right] + \varepsilon, & r_{ij} \le r_{ij}^\mathrm{c} \\ 0, & r_{ij} > r_{ij}^\mathrm{c} \end{cases}, \tag{1}$$

where r_{ij} is the distance between particles i and j, Δ_{ij} is the shift parameter that accounts for size differences between particles of different types, and $r_{ij}^\mathrm{c} = 2^{1/6}\sigma_{ij} + \Delta_{ij}$ is the cutoff distance. For monomer–monomer and NP–NP interactions, $\{\sigma_{ij}, \Delta_{ij}\} = \{\sigma_\mathrm{m}, 0\}$ and $\{\sigma_{ij}, \Delta_{ij}\} = \{\sigma_\mathrm{NP}, 0\}$, respectively. For NP–monomer interactions, $\sigma_{ij} = \sigma_\mathrm{m}$ and

$\Delta_{ij} = (\sigma_{\mathrm{NP}} - \sigma_{\mathrm{m}})/2$.

Bonds between neighboring monomers are modeled using the finitely extensible nonlinear elastic (FENE) potential:[68]

$$U_{\mathrm{FENE}}(r_{ij}) = \begin{cases} -\frac{1}{2} k {r_0}^2 \ln\left[1 - \left(\frac{r_{ij}}{r_0}\right)^2\right], & r_{ij} < r_0 \\ \infty, & r_{ij} \geq r_0 \end{cases}, \tag{2}$$

where $k = 30$ and $r_0 = 1.5$ are the spring constant and maximum bond extension length, respectively. The equilibrium bond length with these parameters is $b \approx 0.97$. The stiffness of rings is controlled by incorporating the bending potential,

$$U_{\mathrm{bend}}(\Theta_{ijk}) = \kappa(1 - \cos\Theta_{ijk}) \tag{3}$$

where Θ_{ijk} is the angle between the bond vectors connecting adjacent monomers $\{i, j\}$ and $\{j, k\}$, and κ is the stiffness parameter.

We examined systems with $N_{\mathrm{m}} = 70$, $\sigma_{\mathrm{m}} = 1$, and $\sigma_{\mathrm{NP}} = 5$. These choices ensure that $\sigma_{\mathrm{NP}} \approx R_{\mathrm{g},0}$ for highly flexible rings ($\kappa \leq 2$), where $R_{\mathrm{g},0}$ is the radius of gyration at infinite dilution (Table 1). To study the influence of ring flexibility, we varied the stiffness parameter $\kappa = 0 - 70$. The NP–polymer solutions were simulated in a cubic cell with edge length $L = 64$, and periodic boundary conditions were applied in all directions. The number of ring polymers N_{P} in the simulation cell was varied from 93 to 1497, yielding solutions with monomer concentrations $c = N_{\mathrm{m}} N_{\mathrm{P}} L^{-3}$ ranging from 0.025 to 0.4 (Table 1). This range of monomer concentrations is well below the typical value $c \approx 0.9$ found in melts of similar polymer models,[36,37,39,53] and thus corresponds to solution-like conditions. At sufficiently high bending stiffness κ, ring polymers can exhibit transitions from isotropic to (discotic) nematic or smectic phases, depending on, e.g., the concentration and ring stiffness.[69] Since we are primarily interested in the transport properties in the isotropic phase, we restrict the maximum monomer concentration (at each investigated κ value) to stay below this phase

transition (Table 1). To model dilute NP conditions, only 20 NPs were simulated in each ring polymer solution, corresponding to an NP volume fraction of approximately 0.005. Using cluster analysis, we confirmed that these conditions are sufficiently dilute to minimize NP–NP interactions and avoid NP aggregation.

Table 1: Properties of semiflexible ring polymer solutions

κ	$R_{g,0}$	c_{min}	c_{max}
0	4.4	0.025 ($0.13c^*$)	0.40 ($2.07c^*$)
1.5	5.0	0.025 ($0.19c^*$)	0.40 ($2.97c^*$)
5	6.8	0.025 ($0.46c^*$)	0.40 ($7.39c^*$)
10	8.5	0.025 ($0.91c^*$)	0.30 ($10.95c^*$)
20	9.7	0.025 ($1.37c^*$)	0.15 ($8.22c^*$)
32	10.1	0.025 ($1.56c^*$)	0.10 ($6.22c^*$)
70	10.5	0.025 ($1.74c^*$)	0.10 ($6.95c^*$)

Notes: c_{min} and c_{max} are the minimum and maximum monomer concentrations investigated in this study, and $c^* = 3N_P(4\pi R_{g,0}^3)^{-1}$ is the overlap concentration.

All simulations were performed at a reduced temperature $T = 1.0$, using a velocity-Verlet scheme with a time step of 0.005 to integrate the equations of motion. The systems were first equilibrated for $\approx 10^6$ time units using Langevin thermostats with LAMMPS "damp" parameters of 3.0 and 0.9 for the NPs and monomers, respectively. This duration is approximately 10 times longer than the relaxation time of the system at the highest κ and c examined, which exhibits the most sluggish dynamics. Next, the systems were simulated using a hybrid MD–MPCD technique to incorporate solvent-mediated HI.[26–28,62] The MPCD parameters and implementation are identical to those employed in our previous studies[26–28] and result in a coarse-grained solvent with dynamic viscosity $\eta_s \approx 4.0$ and Schmidt number $Sc \approx 12$. The NP–polymer solutions were briefly equilibrated for $\approx 5 \times 10^4$ time units with the MD–MPCD scheme to allow the MPCD solvent to thermalize and then simulated for a production period of $\approx 2 \times 10^6$ time units, during which data are collected to compute ensemble averages. Three independent simulations were performed to generate a total of 60 NP trajectories at each set of conditions examined. Static and dynamic properties were calculated by averaging over the independent simulations. Complementary LD simulations

were also performed for select systems using the Langevin thermostats described above to investigate the behavior of the solutions in the absence of many-body HI.

Following our previous study of NP transport in solutions of flexible rings,[28] the polymer mesh size ξ was computed using the geometric pore size distribution defined in Ref. 70. In this method, ξ is calculated as the spatial average of the local pore size $h(\mathbf{r})$, which is defined as the diameter of the largest spherical test probe that can be placed in the polymer system such that it encompasses the point $\mathbf{r}$ without overlapping with the surrounding monomers (points within a distance of 0.5 of a monomer center were considered overlapping). $h(\mathbf{r})$ was evaluated via the non-linear optimization approach described in Refs. 71,72. The resulting ξ provides an unambiguous geometric definition of mesh size that is consistent with intuition for regular polymer networks[72] and is universally applicable regardless of network topology, monomer concentration, or polymer architecture.[28]

3 Results and Discussions

To investigate the dynamics of the NP–polymer solutions, we calculated the mean-squared displacement (MSD) $\langle \Delta r^2 \rangle$ for the monomers in the polymer COM reference frame, for the polymer COM, and for the NPs as a function of the stiffness parameter κ. At short times ($\Delta t < 10^3$), the segmental dynamics of the fully flexible rings ($\kappa = 0$) are hydrodynamically coupled and exhibit $\langle \Delta r^2 \rangle \sim t^{2/3}$ scaling behavior, as predicted by the Zimm model (Fig. 1(a)).[73] Although this scaling behavior is observed for all κ, the magnitude of $\langle \Delta r^2 \rangle$ at a given lag time Δt within this intermediate regime decreases as stiffness increases, indicating a reduction in segmental mobility. This behavior is in agreement with those observed in previous studies of semiflexible linear polymers in solution.[27,74,75] On long times ($\Delta t > 10^4$), the MSD exhibits a terminal plateau $\langle \Delta r^2 \rangle \approx 2R_{g,0}^2$ that arises from the constraints imposed on the monomer motions by their connectivity (Fig. 1(a)). The height of the terminal plateau increases with κ, consistent with stiffer rings exhibiting more expanded conformations and larger $R_{g,0}$ (Table 1).

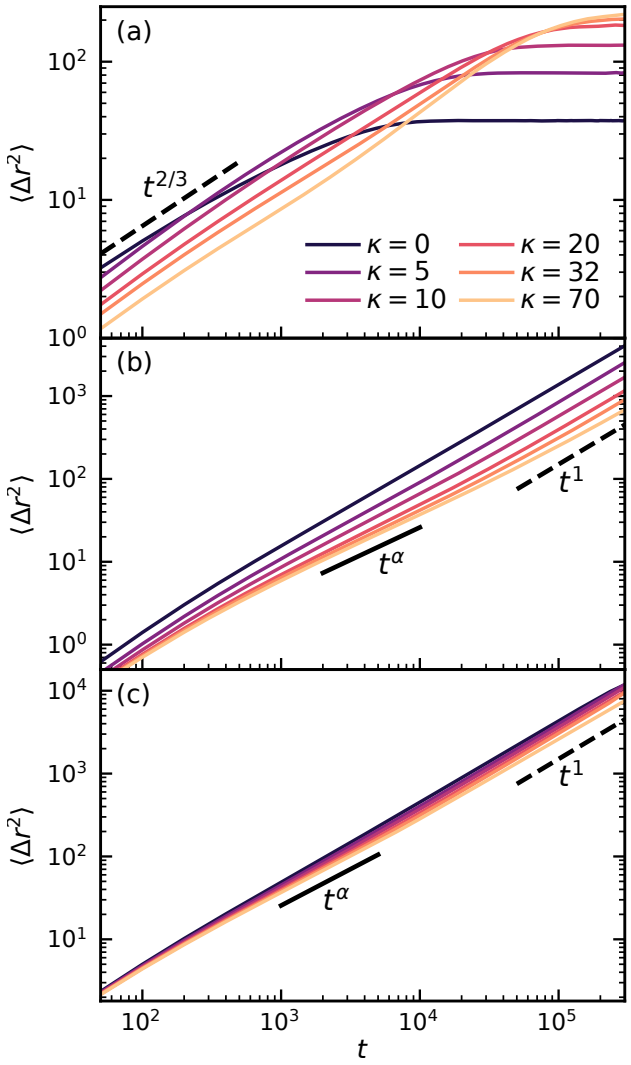

Figure 1: Mean-squared displacements $\langle \Delta r^2 \rangle$ for (a) monomers in the polymer COM reference frame, (b) polymer COM, and (c) the NPs in ring polymer solutions with monomer $c = 0.05$ and different values of the stiffness parameter κ. Dashed line in (a) indicates Zimm ($\sim t^{2/3}$) scaling. Solid and dashed lines in (b) and (c) indicate subdiffusive ($\sim t^\alpha, \alpha < 1$) and diffusive ($\sim t^1$) scaling, respectively.

The polymer COM and NP dynamics are also influenced by ring stiffness. The MSDs for the polymer COM and NPs exhibit subdiffusive behavior on short time scales in which $\langle \Delta r^2 \rangle \sim t^\alpha$ with exponent $\alpha < 1$ but crossover to diffusive dynamics ($\alpha = 1$) on longer time scales. The magnitudes of the MSDs decrease across all time scales with increasing κ, mirroring the slowing of the segmental dynamics. This behavior is consistent with recent simulations of semiflexible ring melts, where a dramatic increase in the zero-shear viscosity

was found with increasing bending stiffness κ.[76] Due to the increase in ring size (i.e., R_g) with κ, the dynamical slowing is more pronounced for the polymer COM than for the NPs, as expected from the SER. These trends are similar to those reported for NPs in solutions of semiflexible linear chains.[27]

3.1 Short-time dynamics

To characterize the effects of ring stiffness on the short-time dynamics, we extracted the subdiffusive exponents α_{NP} and α_P for the NPs and polymer COM from their respective MSDs (Figs. 2). We restrict our range of c and κ to stay in the isotropic phase.[69] The values of α_{NP} and α_P can depend on the range of Δt selected for the analysis. Thus, to avoid ambiguity, we follow Ref. 39 and report the minimum values of α_{NP} and α_P attained in the subdiffusive regime. At low monomer concentration (e.g., $c = 0.025$), α_{NP} gradually decreases with increasing ring stiffness. As the monomer concentration increases, however, the rate of decrease becomes significantly more pronounced. Although subdiffusion can arise from a variety of physical mechanisms including transient caging in glassy colloidal suspensions,[77–80] it is most commonly attributed to a coupling of probe dynamics to viscoelastic relaxations in polymer solutions.[20,30] These relaxations arise from a combination of segmental fluctuations and COM translation of the polymer.[26] Thus, the decrease in α_{NP} with increasing κ and c indicates an enhancement in the strength of the dynamic coupling between particle and polymer dynamics. Indeed, the subdiffusive exponent of the polymer COM α_P exhibits similar qualitative behavior to that of α_{NP} (Fig. 2(b)). A similar decay of α_P with increasing bending stiffness was also observed in previous simulations of pure solutions of semiflexible chains in the semidilute regime.[75]

According to PCT,[30] the dynamics of the NPs depend on the ratio of the NP diameter to polymer mesh size σ_{NP}/ξ. When the NPs are smaller than the mesh size ($\sigma_{NP}/\xi < 1$), their short-time motions are not constrained by the surrounding polymers. As a result, NPs are freely diffusive on all time scales, so the exponent is $\alpha_{NP} = 1$. By contrast, when the NPs are

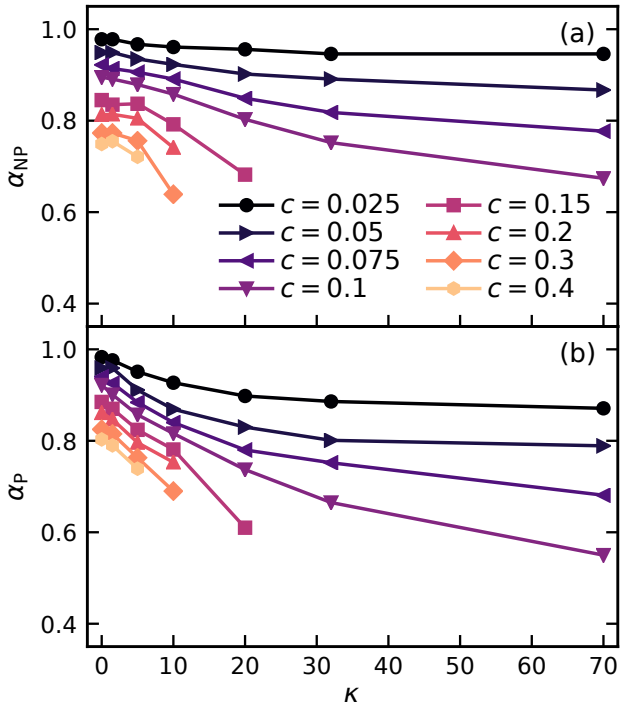

Figure 2: Subdiffusive exponents of the (a) NPs (α_{NP}) and (b) polymer COM (α_P) as functions of stiffness parameter κ for different values of the monomer concentration c.

larger than the mesh size ($\sigma_{NP}/\xi > 1$), they become caged by nearby polymer segments and fully coupled to their relaxations. On length scales larger than ξ, (semi)flexible polymers in semidilute solutions can be regarded as Rouse chains of correlation blobs; the MSD of the polymer segments scales as $\langle \Delta r^2 \rangle \sim t^{1/2}$ at timescales below the Rouse relaxation time,[73,74] leading to an expectation of $\alpha_{NP} = 0.5$.[30] This prediction has been confirmed experimentally for systems in which the NP–polymer dynamics are fully coupled by chemically bonding the NPs to the polymer network.[81] Previous simulations also showed that the NP dynamics are purely diffusive in solutions of free (unpolymerized) monomers at similar values of c.[28] These studies confirm that the NP subdiffusive dynamics, as predicted by PCT, arise from coupling with polymer segmental relaxations with $\alpha_{NP} = 0.5$ in the limit of full coupling.

For the (semi)flexible ring polymer solutions, however, the short-time NP dynamics deviate from PCT predictions (Fig. 3). Rather than abruptly dropping from 1.0 to 0.5 at $\sigma_{NP}/\xi \approx 1$, as predicted by PCT, α_{NP} gradually decreases as σ_{NP}/ξ increases. Similar

deviations from PCT have been reported in experiments on NPs in solutions of linear polymers.[20] They have also been observed in our previous computational work on systems with (semi)flexible linear chains[26,27] and flexible ring polymers.[28] In those previous studies, the faster-than-expected subdiffusive NP dynamics suggested the presence of an additional mode of NP–polymer coupling that is not accounted for in PCT. Indeed, the strong correlation observed between the subdiffusive exponents α_{NP} and α_{P} indicated that the translational COM motions of the NPs and polymers were coupled on short time scales. Thus, these studies suggest that the NP subdiffusive dynamics in solutions of (semi)flexible linear chains and flexible rings are coupled to both the polymer segmental relaxations and their COM motions, whereas only the former coupling mode is described by PCT.

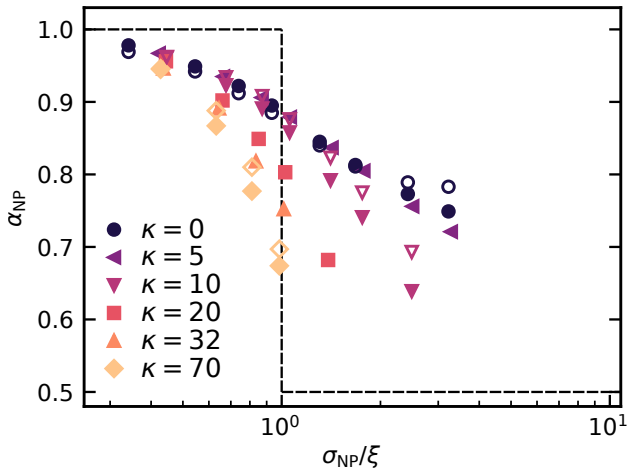

Figure 3: Subdiffusive exponents of the NPs α_{NP} as a function of the ratio of the NP diameter to polymer mesh size σ_{NP}/ξ. Dashed line indicates the prediction from PCT.[30] Closed and open symbols indicate data from hybrid MD–MPCD simulations (with HI) and LD simulations (without HI), respectively.

Interestingly, for the semiflexible ring polymer solutions studied here, we observe that α_{NP} and α_{P} are strongly correlated for all values of κ examined (Fig. 4). Results from complementary LD simulations reveal these correlations are observed even when HI are neglected (Fig. 4). This behavior indicates that the COM motions of the NPs and ring polymers remain coupled even as the rings expand and their segmental dynamics slow as chain stiffness is increased. This finding is in sharp contrast with the behavior observed

in our analogous study of semiflexible *linear* chains, where it was found that α_{NP} and α_P became increasingly decoupled as κ was increased.[27] The decoupling for the linear chains was attributed to them becoming more rod-shaped, leading to increasingly anisotropic polymer COM motions that alter the way in which the NPs and polymers dynamically couple on short time scales. The nature of the NP–ring correlations, however, depends on stiffness, with the NPs being more subdiffusive than polymers at low κ but less subdiffusive at high κ. As discussed below, we attribute this dependence to contributions from structural changes in the polymer solutions.

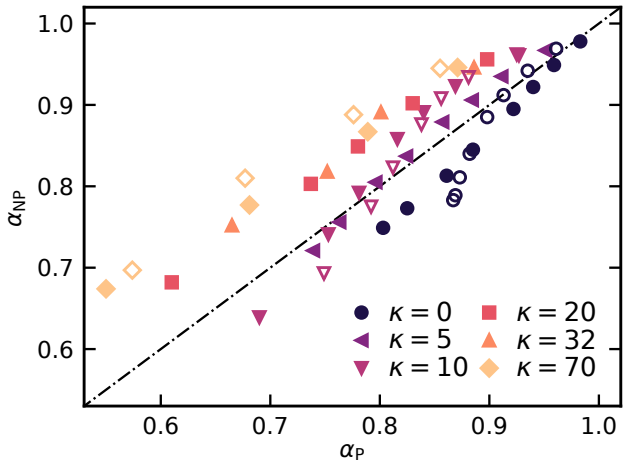

Figure 4: Correlation of NP and polymer COM subdiffusive exponents (α_{NP} and α_P, respectively) for different values of the stiffness parameter κ. Dashed-dotted line indicates $\alpha_{NP} = \alpha_P$. Closed and open symbols indicate data from hybrid MD–MPCD simulations (with HI) and LD simulations (without HI), respectively.

3.2 Long-time dynamics

On longer time scales, both NPs and polymer COMs crossover to diffusive motion with diffusivities (D and D_P, respectively) that decrease monotonically with increasing κ and c. These trends match those observed for the subdiffusive exponents (Fig. 5), indicating that the slowing of the segmental dynamics and changes in ring conformations upon increasing bending stiffness (see Sec. 3.3) affect both the short- and long-time translational dynamics of the NPs and polymer COM. Indeed, PCT assumes that the polymer segments surrounding

the NPs present an infinite energy barrier to diffusion and that the segments must relax before the NPs can escape their local cages. Specifically, PCT asserts that the segments must relax over length scales comparable to the NP diameter, resulting in the scaling prediction $D/D_0 \sim (\sigma_{\mathrm{NP}}/\xi)^{\gamma}$ with exponent $\gamma = -2$ for $\sigma_{\mathrm{NP}}/\xi \geq 1$, where D_0 is the NP diffusivity in the background solvent.

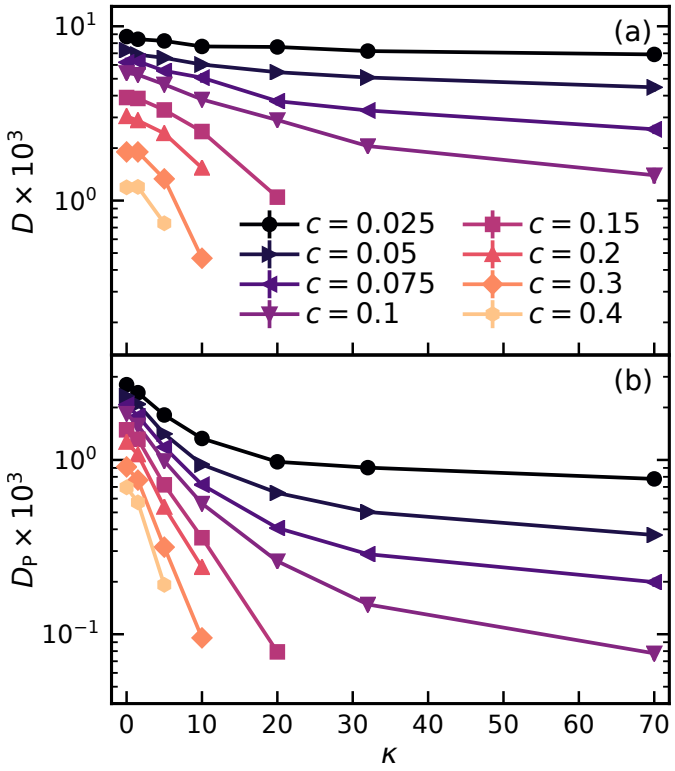

Figure 5: Diffusion coefficients of the (a) NPs (D) and (b) polymer COM (D_{P}) as functions of stiffness parameter κ for various monomer concentrations c.

The PCT scaling predicting for D/D_0 has been confirmed in experimental[20] and computational studies[26] of NP diffusion in solutions of flexible linear chains; it has also been found to be approximately consistent with results from simulations of flexible ring polymers.[28] We observe that D/D_0 decreases with σ_{NP}/ξ for $\sigma_{\mathrm{NP}}/\xi \geq 1$. Although this decreasing trend is generally consistent with PCT, it is not possible to determine whether the decay follows power-law behavior with the predicted scaling exponent of $\gamma = -2$ due to the limited range of σ_{NP}/ξ accessible for these systems. The decrease in NP diffusivity starts at smaller σ_{NP}/ξ with increasing κ, indicating that the NPs more readily experience local heterogeneities for

stiffer rings. As κ increases, the segmental dynamics slow and the time scale for the polymer segments to relax over the NP surfaces increases. Hence, we posit that this slowing results in a sharper decrease in D/D_0 as the mesh size decreases and the NPs become more confined by the surrounding polymers. Langevin dynamics simulations show that these qualitative trends are largely insensitive to the inclusion of many-body HI, which is consistent with our previous computational study of NPs in solutions of flexible linear chains.[26] Lastly, we observe that the terminal NP and polymer COM diffusivites are approximately linearly correlated for all κ examined (Fig. 7). The linear correlation is consistent with the terminal NP and polymer COM motions being strongly coupled to the bulk solution viscosity. In the limit of full coupling, the SER would predict that $D/D_\mathrm{P} \propto R_\mathrm{g}/\sigma_\mathrm{NP}$. Accordingly, we find that the slope of D versus D_P increases as κ increases due to the concomitant increase in ring size (i.e., increase in R_g).

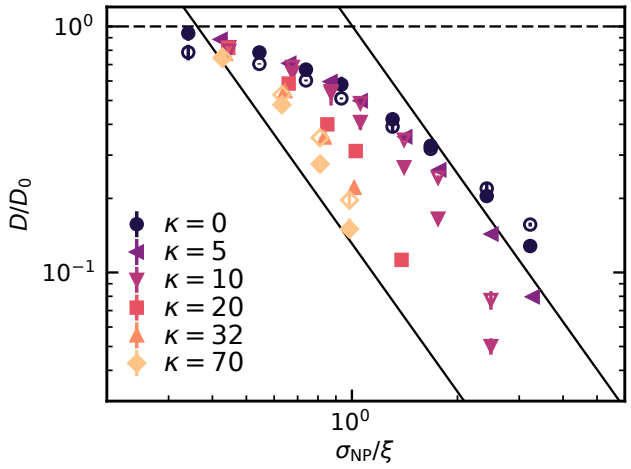

Figure 6: Normalized diffusivity of NPs D/D_0 as a function of ratio NP size and polymer mesh size σ_NP/ξ. The solid lines denote the $D/D_0 \sim (\sigma_\mathrm{NP}/\xi)^{-2}$ scaling behavior predicted by PCT.[30] Closed and open symbols indicate data from hybrid MD–MPCD simulations (with HI) and LD simulations (without HI), respectively.

3.3 Structural effects

The observed changes to NP dynamics over short and long time scales indicate a unique coupling to local heterogeneities in solutions of stiff rings. We therefore characterized structural

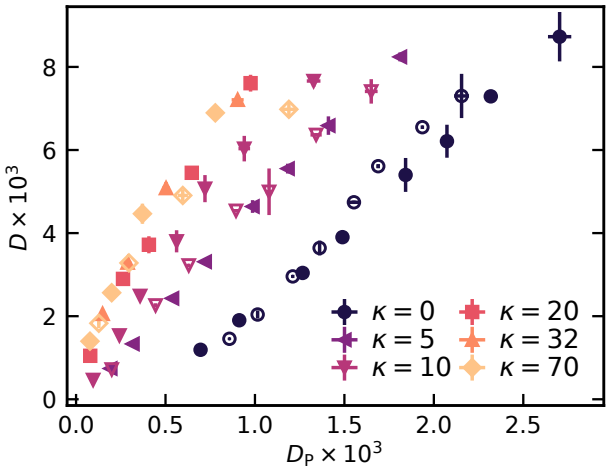

Figure 7: Correlation of terminal NP and polymer COM diffusivities (D and D_{P}, respectively) for different values of the stiffness parameter κ. Closed and open symbols indicate data from hybrid MD–MPCD simulations (with HI) and LD simulations (without HI), respectively.

properties of the solutions to understand their potential influence on the NP and polymer dynamics. To this end, we first analyzed the shape of the individual polymers by computing the gyration tensor

$$G_{\alpha\beta} = \frac{1}{N_{\mathrm{m}}} \sum_i (\Delta r_{i,\alpha} \Delta r_{j,\beta}). \tag{4}$$

where $\Delta r_{i,\alpha}$ is the position of monomer i relative to the polymer COM, and α and β denote components along the Cartesian x, y, and z directions. Several descriptors can be calculated from the gyration tensor, including the radius of gyration

$$R_{\mathrm{g}} = (\lambda_1 + \lambda_2 + \lambda_3)^{1/2}, \tag{5}$$

where $\lambda_1 > \lambda_2 > \lambda_3$ are the eigenvalues of the gyration tensor. The polymer shape can be characterized via the asphericity,

$$a = \frac{(\lambda_1 - \lambda_2)^2 + (\lambda_2 - \lambda_3)^2 + (\lambda_3 - \lambda_1)^2}{2(\lambda_1 + \lambda_2 + \lambda_3)^2}, \tag{6}$$

which has limiting values of 0 and 1 for perfectly spherical ($\lambda_1 = \lambda_2 = \lambda_3$) and one-dimensional objects ($\lambda_2 = \lambda_3 = 0$), respectively. For a three-dimensional random walk with $N_\mathrm{m} \to \infty$, numerical calculations have found $a = 0.039$.[82] For polymers with $a > 0$, the nature of their asphericity can further be characterized using the prolateness,

$$p = \frac{(2\lambda_1 - \lambda_2 - \lambda_3)(2\lambda_2 - \lambda_3 - \lambda_1)(2\lambda_3 - \lambda_1 - \lambda_2)}{2(\lambda_1^2 + \lambda_2^2 + \lambda_3^2 - \lambda_1\lambda_2 - \lambda_2\lambda_3 - \lambda_3\lambda_1)^{3/2}}, \tag{7}$$

which has limiting values of 1 and -1 for perfectly prolate (rod-like) and oblate (disk-like) objects, respectively.

The shape descriptors R_g, a, and p exhibit weak variations with monomer concentration c (Fig. 8). Specifically, the R_g of rings with $\kappa \leq 5$ decreases by about 15% as the concentration increases from $c = 0.025$ to $c = 0.4$. This behavior aligns with the expected transition from good solvent conditions in dilute solutions to theta-like conditions above the overlap concentration (Table 1).[83,84] This effect becomes much weaker with increasing κ, however, because the conformations of stiff rings are primarily dictated by the intramolecular bending energy and packing entropy.[85–88] The radius of gyration R_g increases monotonically with κ, exhibiting an initial sharp rise over the range $0 \leq \kappa \leq 10$ followed by a much smaller growth for $\kappa \gtrsim 20$. The expansion of the rings is accompanied by nonmonotonic changes in the shape descriptors a and p, which both initially increase and then decrease for $\kappa \geq 10$. The sign of p changes from positive to negative at $\kappa \approx 20$, indicating that rings transition from prolate- to oblate-like objects as κ increases. Whereas the probability density distributions for R_g and a exhibit well-defined maxima for all κ, $P(p)$ becomes almost flat at $\kappa = 20$ (Fig. 9). This behavior reveals that fluctuations in p are maximized near $\kappa = 20$ and that the mean value of $p \approx 0$ results from averaging over the nearly uniform $P(p)$ distribution at this critical value of the stiffness parameter.

The changes in ring structure with κ also affect the structural correlations between the NP–polymer and polymer–polymer COM, as measured by the respective radial distribution

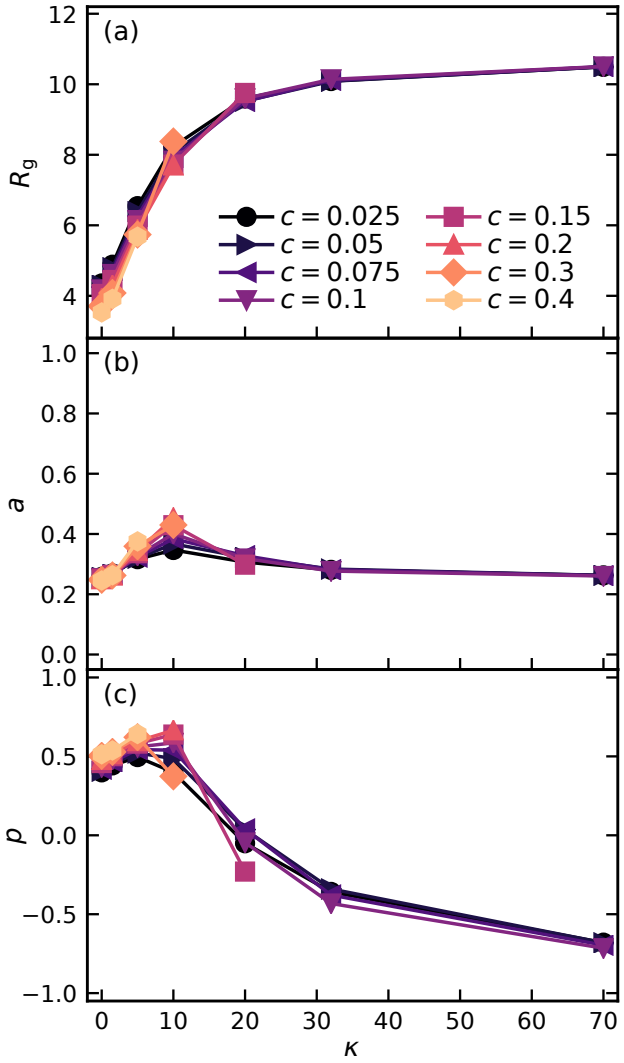

Figure 8: (a) Radius of gyration R_g, (b) asphericity a, and (c) prolateness p of the ring polymers as function of stiffness parameter κ for different monomer concentrations c.

functions (RDFs) $g_{\mathrm{NP-P}}(r)$ and $g_{\mathrm{P-P}}(r)$ (Fig. 10). The RDFs for the solutions with fully flexible rings ($\kappa = 0$) are approximately zero for $r \leq 5$ and exhibit single maxima in the range $r \approx 8{-}10 \approx 2R_g$ before decaying towards unity at larger r. The compact and isotropic nature of the flexible rings results in effective short-ranged excluded volume interactions between the NP–polymer and polymer–polymer COM, which prevent them from coming into close proximity and lead to the formation of well-defined neighbor contact peaks in $g_{\mathrm{NP-P}}(r)$ and $g_{\mathrm{P-P}}(r)$ at intermediate $r \approx \sigma_{\mathrm{NP}} + R_g$ and $r \approx 2R_g$, respectively. The RDF $g_{\mathrm{NP-P}}(r)$ for semiflexible rings with $\kappa = 10$, by contrast, is nearly flat except for a slight upturn near

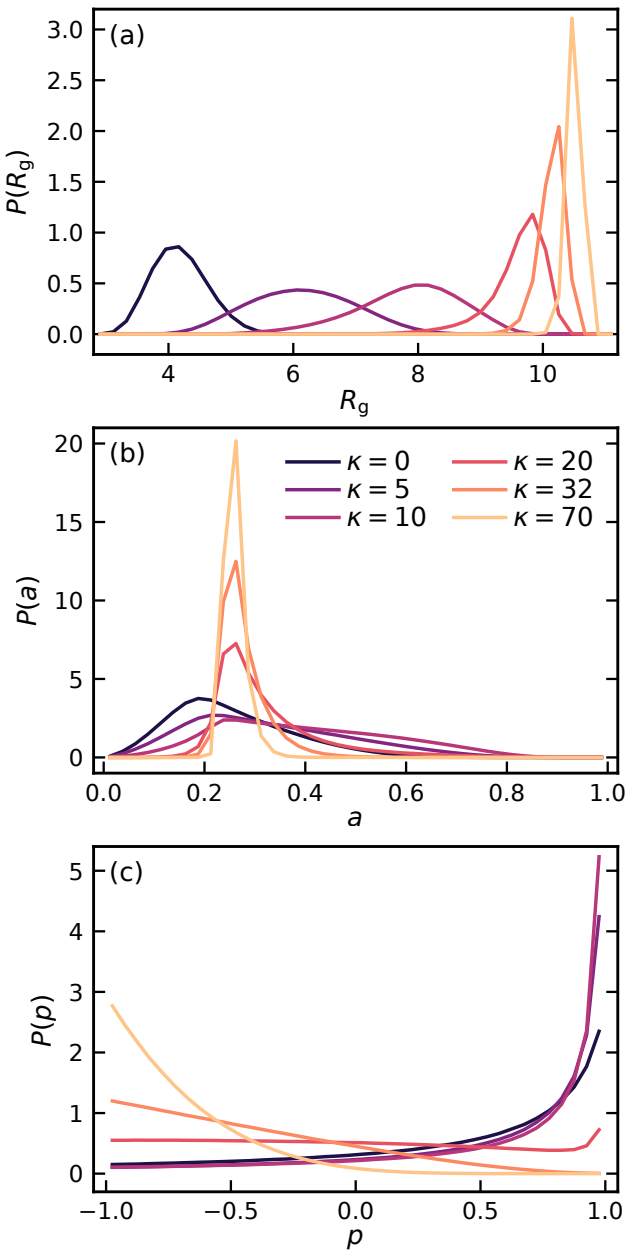

Figure 9: Probability density distributions of the (a) radius of gyration R_g, (b) asphericity a, and (c) prolateness p of the ring polymers at monomer concentration $c = 0.1$ for different values of the stiffness parameter κ.

$r = 0$. This behavior suggests that the effective excluded volume interaction between the NP and polymer COM vanishes, allowing a small fraction of the NPs to penetrate the center of the rings such that the positions of their COM coincide. A similar interpenetration or "threading" of the rings explains the increase in $g_{\mathrm{P-P}}(r)$ at $r = 0$.[85–88] Interestingly, $g_{\mathrm{NP-P}}$

and $g_{\mathrm{P-P}}(r)$ both flatten at $\kappa = 10$, where the distributions of the ring shape descriptors R_{g}, a, and p are also relatively broad (Fig. 9). This behavior suggests that large fluctuations in ring shape allow interpenetration to occur, reducing excluded volume effects such that the NP–polymer and polymer–polymer interactions become nearly ideal under these conditions.

As κ increases further, the rings continue to expand and become increasingly oblate. These conformational changes coincide with $g_{\mathrm{NP-P}}(r)$ increasing in magnitude at low r and developing a strong peak at $r = 0$. Similar trends are observed in $g_{\mathrm{P-P}}(r)$ along with the formation of a second peak at $r \approx 3$. Inspection of configurations from the simulations confirm that the peaks at $r = 0$ signify an increased propensity for NPs and polymers to occupy the "holes" created in the centers of the rings as they stiffen and expand (Figs. 10(b) and 11). They also reveal that the second peak observed in $g_{\mathrm{P-P}}(r)$ at $r \approx 3$ arises from the local ordering of neighboring rings into stacked arrangements (Fig. 10(b)).[76,85,87]

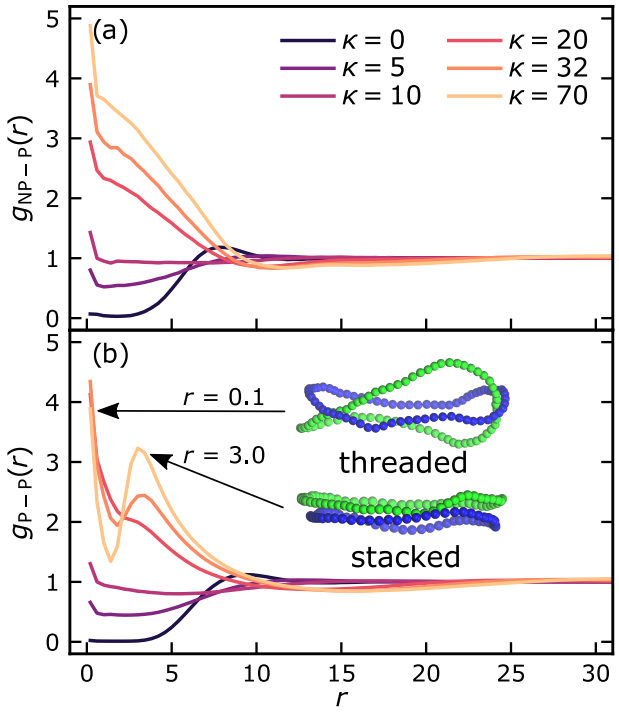

Figure 10: Radial distribution functions for the (a) NP–polymer COM and (b) polymer–polymer COM at monomer concentration $c = 0.1$ for different values of the stiffness parameter κ. The inset in (b) shows the threaded and stacked ring arrangements observed for $\kappa = 70$ at $r \approx 0.1$ and $r \approx 3.0$, respectively.

We posit that the ring conformational changes observed upon varying κ directly influence the caging of the NPs. Specifically, the compact conformations of flexible rings have characteristic dimensions similar to those of the NPs, allowing the rings to behave as soft crowders that transiently cage the NPs. Consequently, the short-time NP dynamics couple to the ring segmental relaxations and translational COM motions. As κ increases, the polymers expand and the segmental relaxations slow. In the case of semiflexible linear chains, chain stiffening causes the polymer COM motions to become increasingly anisotropic and decoupled from the NP dynamics. For semiflexible rings, by contrast, the short-time NP and polymer COM dynamics remain strongly coupled due to transient caging of the NPs inside the "holes" near the ring centers as they adopt more expanded conformations. Thus, although the NPs experience distinct local environments when caged by flexible rings with compact conformations or within semiflexible rings with expanded conformations, both types of cages lead to strong coupling of the NP and polymer COM dynamics on short time scales. As a result, coupling of NP and polymer subdiffusive dynamics is observed across the full range of κ examined.

4 Conclusions

We used hybrid MD–MPCD simulations to investigate the diffusion of NPs in solutions of ring polymers with tunable stiffness. The NPs exhibit subdiffusive dynamics on short time scales before transitioning to normal diffusion at longer times. The NP diffusivity decreases as the ratio of the NP diameter to polymer mesh size σ_{NP}/ξ becomes sufficiently large. Although this decreasing trend is generally consistent with PCT, it is not possible to determine whether the decay follows the predicted power-law behavior due to the limited range of σ_{NP}/ξ accessible for these systems. The NP subdiffusive exponents in solutions of flexible rings are larger than those predicted by PCT and strongly correlated with those of the polymer COM. These findings mirror those reported for NPs in solutions of flexible linear chains,[26] which exhibit similar dynamics to solutions of flexible ring polymers when compared at the same monomer concentration.[28] The faster-than-predicted subdiffusive dynamics in

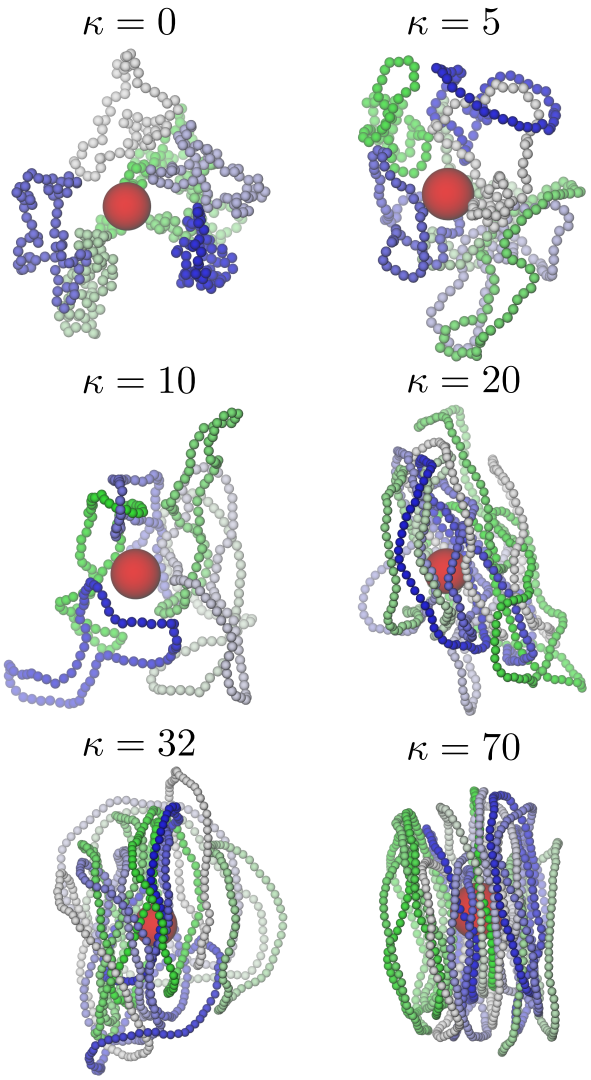

Figure 11: Ring polymers (chains of small spheres) around a central NP (large red sphere) at monomer concentration $c = 0.1$ for different values of the stiffness parameter κ. Only rings whose COM are within a separation distance of $r = 10$ from that of the central NP are shown. Snapshots are rendered using Visual Molecular Dynamics 1.9.3.[89]

.

both cases arises from coupling between the NP and polymer COM motions on short time scales, which is not accounted for by PCT.

As the rings become stiffer, the terminal NP diffusivity decreases. The short-time dynamics of the NPs also become slower, as evidenced by the decrease in their subdiffusive exponent. These trends are reminiscent of those reported for solutions of semiflexible linear chains and are attributed the reduced segmental mobility of stiff polymers.[27] Interestingly,

the NP and ring polymer COM subdiffusive exponents remain strongly correlated for all of the examined semiflexible ring polymer solutions. This behavior is at odds with the pronounced decoupling of the NP and polymer COM motions observed upon increasing the stiffness of linear chains.[27] Our analysis indicates that stiffer ring polymers adopt increasingly circular conformations, accompanied by a distinct stacking into transient tubes. The void space created near the ring centers is occupied by NPs and other polymers, resulting in a strong coupling on short time scales between the dynamics of NPs and those of the polymer centers-of-mass. These insights identify the unique transport properties of NPs in semidilute solutions of ring polymers and serve as a starting model by which to predict transport in (bio)macromolecule suspensions[36–42] and, in future work, uncover the microstructural origins of the coupling across broad ranges of particle and polymer size.

Acknowledgement

This work was supported by the Welch Foundation (Grants E-1882, E-1869, and the Welch Center for Advanced Bioactive Materials Crystallization, Award V-E-0001), the National Science Foundation (CBET-2004652, CBET-1803728, and CBET-2223084), the ACS Petroleum Research Fund (65826-DNI9), and the Deutsche Forschungsgemeinschaft (DFG, German Research Foundation, Project No. 470113688). Computational resources were provided by the Hewlett Packard Enterprise Data Science Institute at the University of Houston and the Texas Advanced Computing Center at the University of Texas at Austin.

References

(1) Shamsijazeyi, H.; Miller, C. A.; Wong, M. S.; Tour, J. M.; Verduzco, R. Polymer-coated nanoparticles for enhanced oil recovery. *J. Appl. Polym. Sci.* **2014**, *131*, 40576.

(2) Soppimath, K. S.; Aminabhavi, T. M.; Kulkarni, A. R.; Rudzinski, W. E. Biodegradable polymeric nanoparticles as drug delivery devices. *J. Control. Release* **2001**, *70*, 1–20.

(3) Liechty, W. B.; Kryscio, D. R.; Slaughter, B. V.; Peppas, N. A. Polymers for drug delivery systems. *Annu. Rev. Chem. Biomol. Eng.* **2010**, *1*, 149–173.

(4) Tang, L.; Yang, X.; Yin, Q.; Cai, K.; Wang, H.; Chaudhury, I.; Yao, C.; Zhou, Q.; Kwon, M.; Hartman, J. A.; Dobrucki, I. T.; Dobrucki, L. W.; Borst, L. B.; Lezmi, S.; Helferich, W. G.; Ferguson, A. L.; Fan, T. M.; Cheng, J. Investigating the optimal size of anticancer nanomedicine. *Proc. Natl. Acad. Sci.* **2014**, *111*, 15344–15349.

(5) Blanco, E.; Shen, H.; Ferrari, M. Principles of nanoparticle design for overcoming biological barriers to drug delivery. *Nat. Biotechnol.* **2015**, *33*, 941.

(6) Barua, S.; Mitragotri, S. Challenges associated with penetration of nanoparticles across cell and tissue barriers: A review of current status and future prospects. *Nano Today* **2014**, *9*, 223–243.

(7) Poon, W.; Kingston, B. R.; Ouyang, B.; Ngo, W.; Chan, W. C. A framework for designing delivery systems. *Nature Nanotechnology* **2020**, *15*, 819–829.

(8) Hanemann, T.; Szabó, D. V. Polymer-nanoparticle composites: from synthesis to modern applications. *Materials* **2010**, *3*, 3468–3517.

(9) Chen, Q.; Gong, S.; Moll, J.; Zhao, D.; Kumar, S. K.; Colby, R. H. Mechanical reinforcement of polymer nanocomposites from percolation of a nanoparticle network. *ACS Macro Lett.* **2015**, *4*, 398–402.

(10) Sarkar, B.; Alexandridis, P. Block copolymer-nanoparticle composites: structure, functional properties, and processing. *Prog. Polym. Sci.* **2015**, *40*, 33–62.

(11) Bailey, E. J.; Winey, K. I. Dynamics of polymer segments, polymer chains, and nanoparticles in polymer nanocomposite melts: A review. *Progress in Polymer Science* **2020**, *105*, 101242.

(12) Nepal, D.; Haines, J.; Vaia, R. A. Polymer nanocomposites: 35 years on. *MRS Bulletin* **2023**, *49*, 236–246.

(13) Lee, B. J.; Cheema, Y.; Bader, S.; Duncan, G. A. Shaping nanoparticle diffusion through biological barriers to drug delivery. *JCIS Open* **2021**, *4*, 100025.

(14) Mason, T. G.; Weitz, D. A. Optical measurements of frequency-dependent linear viscoelastic moduli of complex fluids. *Phys. Rev. Lett.* **1995**, *74*, 1250.

(15) Mason, T. G.; Gisler, T.; Kroy, K.; Frey, E.; Weitz, D. A. Rheology of F-actin solutions determined from thermally driven tracer motion. *J. Rheol.* **2000**, *44*, 917–927.

(16) Ye, X.; Tong, P.; Fetters, L. J. Transport of probe particles in semidilute polymer solutions. *Macromolecules* **1998**, *31*, 5785–5793.

(17) Cheng, Y.; Prud'homme, R. K.; Thomas, J. L. Diffusion of mesoscopic probes in aqueous polymer solutions measured by fluorescence recovery after photobleaching. *Macromolecules* **2002**, *35*, 8111–8121.

(18) Tuteja, A.; Mackay, M. E.; Narayanan, S.; Asokan, S.; Wong, M. S. Breakdown of the continuum Stokes-Einstein relation for nanoparticle diffusion. *Nano Lett.* **2007**, *7*, 1276–1281.

(19) Kohli, I.; Mukhopadhyay, A. Diffusion of nanoparticles in semidilute polymer solutions: effect of different length scales. *Macromolecules* **2012**, *45*, 6143–6149.

(20) Poling-Skutvik, R.; Krishnamoorti, R.; Conrad, J. C. Size-dependent dynamics of nanoparticles in unentangled polyelectrolyte solutions. *ACS Macro Lett.* **2015**, *4*, 1169–1173.

(21) Ge, T. Scaling Perspective on Dynamics of Nanoparticles in Polymers: Length- and Time-Scale Dependent Nanoparticle–Polymer Coupling. *Macromolecules* **2023**, *56*, 3809–3837.

(22) Kalathi, J. T.; Grest, G. S.; Kumar, S. K. Universal Viscosity Behavior of Polymer Nanocomposites. *Phys. Rev. Lett.* **2012**, *109*, 198301.

(23) Kalathi, J. T.; Yamamoto, U.; Schweizer, K. S.; Grest, G. S.; Kumar, S. K. Nanoparticle Diffusion in Polymer Nanocomposites. *Phys. Rev. Lett.* **2014**, *112*, 108301.

(24) Chen, A.; Zhao, N.; Hou, Z. The effect of hydrodynamic interactions on nanoparticle diffusion in polymer solutions: a multi-particle collision dynamics study. *Soft Matter* **2017**, *13*, 8625–8635.

(25) Sorichetti, V.; Hugouvieux, V.; Kob, W. Structure and dynamics of a polymer-nanoparticle composite: Effect of nanoparticle size and volume fraction. *Macromolecules* **2018**, *51*, 5375–5391.

(26) Chen, R.; Poling-Skutvik, R.; Nikoubashman, A.; Howard, M. P.; Conrad, J. C.; Palmer, J. C. Coupling of nanoparticle dynamics to polymer center-of-mass motion in semidilute polymer solutions. *Macromolecules* **2018**, *51*, 1865–1872.

(27) Chen, R.; Poling-Skutvik, R.; Howard, M. P.; Nikoubashman, A.; Egorov, S. A.; Conrad, J. C.; Palmer, J. C. Influence of polymer flexibility on nanoparticle dynamics in semidilute solutions. *Soft Matter* **2019**, *15*, 1260–1268.

(28) Chen, R.; Kotkar, S. B.; Poling-Skutvik, R.; Howard, M. P.; Nikoubashman, A.; Conrad, J. C.; Palmer, J. C. Nanoparticle dynamics in semidilute polymer solutions: Rings versus linear chains. *Journal of Rheology* **2021**, *65*, 745–755.

(29) Lin, T.-W.; Mei, B.; Schweizer, K. S.; Sing, C. E. Simulation study of the effects

of polymer network dynamics and mesh confinement on the diffusion and structural relaxation of penetrants. *The Journal of Chemical Physics* **2023**, *159*, 014904.

(30) Cai, L.-H.; Panyukov, S.; Rubinstein, M. Mobility of nonsticky nanoparticles in polymer liquids. *Macromolecules* **2011**, *44*, 7853–7863.

(31) Egorov, S. A. Anomalous nanoparticle diffusion in polymer solutions and melts: A mode-coupling theory study. *J. Chem. Phys.* **2011**, *134*, 84903.

(32) Dell, Z. E.; Schweizer, K. S. Theory of Localization and Activated Hopping of Nanoparticles in Cross-Linked Networks and Entangled Polymer Melts. *Macromolecules* **2014**, *47*, 405–414.

(33) Cai, L.-H.; Panyukov, S.; Rubinstein, M. Hopping Diffusion of Nanoparticles in Polymer Matrices. *Macromolecules* **2015**, *48*, 847–862.

(34) Dong, Y.; Feng, X.; Zhao, N.; Hou, Z. Diffusion of nanoparticles in semidilute polymer solutions: A mode-coupling theory study. *J. Chem. Phys.* **2015**, *143*, 024903.

(35) Yamamoto, U.; Schweizer, K. S. Microscopic Theory of the Long-Time Diffusivity and Intermediate-Time Anomalous Transport of a Nanoparticle in Polymer Melts. *Macromolecules* **2015**, *48*, 152–163.

(36) Halverson, J. D.; Lee, W. B.; Grest, G. S.; Grosberg, A. Y.; Kremer, K. Molecular dynamics simulation study of nonconcatenated ring polymers in a melt. I. Statics. *J. Chem. Phys.* **2011**, *134*, 204904.

(37) Halverson, J. D.; Lee, W. B.; Grest, G. S.; Grosberg, A. Y.; Kremer, K. Molecular dynamics simulation study of nonconcatenated ring polymers in a melt. II. Dynamics. *J. Chem. Phys.* **2011**, *134*, 204905.

(38) Ge, T.; Panyukov, S.; Rubinstein, M. Self-similar conformations and dynamics in entangled melts and solutions of nonconcatenated ring polymers. *Macromolecules* **2016**, *49*, 708–722.

(39) Ge, T.; Kalathi, J. T.; Halverson, J. D.; Grest, G. S.; Rubinstein, M. Nanoparticle motion in entangled melts of linear and nonconcatenated ring polymers. *Macromolecules* **2017**, *50*, 1749–1754.

(40) Brown, S.; Szamel, G. Structure and dynamics of ring polymers. *J. Chem. Phys.* **1998**, *108*, 4705–4708.

(41) Gagliardi, S.; Arrighi, V.; Dagger, A.; Semlyen, A. Conformation of cyclic and linear polydimethylsiloxane in the melt: a small-angle neutron-scattering study. *Appl. Phys. A* **2002**, *74*, s469–s471.

(42) Beaucage, G.; Kulkarni, A. S. Dimensional description of cyclic macromolecules. *Macromolecules* **2009**, *43*, 532–537.

(43) Robertson, R. M.; Smith, D. E. Strong effects of molecular topology on diffusion of entangled DNA molecules. *Proc. Natl. Acad. Sci. USA* **2007**, *104*, 4824–4827.

(44) Kapnistos, M.; Lang, M.; Vlassopoulos, D.; Pyckhout-Hintzen, W.; Richter, D.; Cho, D.; Chang, T.; Rubinstein, M. Unexpected power-law stress relaxation of entangled ring polymers. *Nat. Mater.* **2008**, *7*, 997.

(45) Rosa, A.; Orlandini, E.; Tubiana, L.; Micheletti, C. Structure and Dynamics of Ring Polymers: Entanglement Effects Because of Solution Density and Ring Topology. *Macromolecules* **2011**, *44*, 8668–8680.

(46) Goossen, S.; Brás, A.; Krutyeva, M.; Sharp, M.; Falus, P.; Feoktystov, A.; Gasser, U.; Pyckhout-Hintzen, W.; Wischnewski, A.; Richter, D. Molecular scale dynamics of large ring polymers. *Phys. Rev. Lett.* **2014**, *113*, 168302.

(47) Soh, B. W.; Klotz, A. R.; Robertson-Anderson, R. M.; Doyle, P. S. Long-Lived Self-Entanglements in Ring Polymers. *Phys. Rev. Lett.* **2019**, *123*, 048002.

(48) Gartner, T. E.; Haque, F. M.; Gomi, A. M.; Grayson, S. M.; Hore, M. J. A.; Jayaraman, A. Scaling Exponent and Effective Interactions in Linear and Cyclic Polymer Solutions: Theory, Simulations, and Experiments. *Macromolecules* **2019**, *52*, 4579–4589.

(49) Zhou, Y.; Hsiao, K.-W.; Regan, K. E.; Kong, D.; McKenna, G. B.; Robertson-Anderson, R. M.; Schroeder, C. M. Effect of molecular architecture on ring polymer dynamics in semidilute linear polymer solutions. *Nat. Commun.* **2019**, *10*, 1753.

(50) Weiss, L. B.; Likos, C. N.; Nikoubashman, A. Spatial Demixing of Ring and Chain Polymers in Pressure-Driven Flow. *Macromolecules* **2019**, *52*, 7858–7869.

(51) Obukhov, S. P.; Rubinstein, M.; Duke, T. Dynamics of a ring polymer in a gel. *Phys. Rev. Lett.* **1994**, *73*, 1263.

(52) Michieletto, D.; Turner, M. S. A topologically driven glass in ring polymers. *Proceedings of the National Academy of Sciences* **2016**, *113*, 5195–5200.

(53) Ge, T.; Grest, G. S.; Rubinstein, M. Nanorheology of Entangled Polymer Melts. *Phys. Rev. Lett.* **2018**, *120*, 057801.

(54) Zhou, X.; Jiang, Y.; Chen, J.; He, L.; Zhang, L. Size-dependent nanoparticle dynamics in semiflexible ring polymer nanocomposites. *Polymer* **2017**, *131*, 243 – 251.

(55) Nahali, N.; Rosa, A. Nanoprobe diffusion in entangled polymer solutions: Linear vs. unconcatenated ring chains. *J. Chem. Phys.* **2018**, *148*, 194902.

(56) Yue, T.; Zhao, H.; Wei, Y.; Duan, P.; Zhang, L.; Wang, J.; Liu, J. Influence of Nanoparticles on the Structure, Dynamics, and Mechanical Behavior of Nonconcatenated Ring Polymers. *Macromolecules* **2024**, *57*, 1207–1219.

(57) Zimmermann, S. B.; Trach, S. O. Estimation of macromolecule concentrations and excluded volume effects for the cytoplasm of Escherichia coli. *J. Mol. Biol.* **1991**, *222*, 599.

(58) Weiss, M.; Elsner, M.; Kartberg, F.; Nilsson, T. Anomalous Subdiffusion Is a Measure for Cytoplasmic Crowding in Living Cells. *Biophys. J.* **2004**, *87*, 3518–3524.

(59) Mika, J. T.; Poolman, B. Macromolecule diffusion and confinement in prokaryotic cells. *Curr. Opin. Biotechnol.* **2011**, *22*, 117–126.

(60) Dünweg, B.; Kremer, K. Molecular dynamics simulation of a polymer chain in solution. *J. Chem. Phys.* **1993**, *99*, 6983–6997.

(61) Huang, C.-C.; Winkler, R. G.; Sutmann, G.; Gompper, G. Semidilute polymer solutions at equilibrium and under shear flow. *Macromolecules* **2010**, *43*, 10107–10116.

(62) Howard, M. P.; Nikoubashman, A.; Palmer, J. C. Modeling hydrodynamic interactions in soft materials with multiparticle collision dynamics. *Curr. Opin. Chem. Eng.* **2019**, *23*, 34–43.

(63) Hsiao, K.-W.; Schroeder, C. M.; Sing, C. E. Ring Polymer Dynamics Are Governed by a Coupling between Architecture and Hydrodynamic Interactions. *Macromolecules* **2016**, *49*, 1961–1971.

(64) Malevanets, A.; Kapral, R. Mesoscopic model for solvent dynamics. *J. Chem. Phys.* **1999**, *110*, 8605–8613.

(65) Gompper, G.; Ihle, T.; Kroll, D. M.; Winkler, R. G. *Adv. Comput. Simul. Approaches Soft Matter Sci. III*; Springer, 2009; pp 1–87.

(66) Plimpton, S. Fast parallel algorithms for short-range molecular dynamics. *J. Comput. Phys.* **1995**, *117*, 1–19.

(67) Weeks, J. D.; Chandler, D.; Andersen, H. C. Role of repulsive forces in determining the equilibrium structure of simple liquids. *J. Chem. Phys.* **1971**, *54*, 5237–5247.

(68) Grest, G. S.; Kremer, K. Molecular dynamics simulation for polymers in the presence of a heat bath. *Phys. Rev. A* **1986**, *33*, 3628.

(69) Avendaño, C.; Jackson, G.; Müller, E. A.; Escobedo, F. A. Assembly of porous smectic structures formed from interlocking high-symmetry planar nanorings. *Proc. Natl. Acad. Sci. USA* **2016**, *113*, 9699–9703.

(70) Gelb, L. D.; Gubbins, K. E. Pore Size Distributions in Porous Glasses: A Computer Simulation Study. *Langmuir* **1999**, *15*, 305–308.

(71) Bhattacharya, S.; Gubbins, K. E. Fast Method for Computing Pore Size Distributions of Model Materials. *Langmuir* **2006**, *22*, 7726–7731.

(72) Sorichetti, V.; Hugouvieux, V.; Kob, W. Determining the Mesh Size of Polymer Solutions via the Pore Size Distribution. *Macromolecules* **2020**, *53*, 2568–2581.

(73) Doi, M.; Edwards, S. F. *The theory of polymer dynamics*; Clarendon Press, Oxford, 1986.

(74) Nikoubashman, A.; Milchev, A.; Binder, K. Dynamics of single semiflexible polymers in dilute solution. *J. Chem. Phys.* **2016**, *145*, 234903.

(75) Nikoubashman, A.; Howard, M. P. Equilibrium Dynamics and Shear Rheology of Semiflexible Polymers in Solution. *Macromolecules* **2017**, *50*, 8279–8289.

(76) Datta, R.; Berressem, F.; Schmid, F.; Nikoubashman, A.; Virnau, P. Viscosity of Flexible and Semiflexible Ring Melts: Molecular Origins and Flow-Induced Segregation. *Macromolecules* **2023**, *56*, 7247–7255.

(77) Van Megen, W.; Underwood, S. M. Dynamic-Light-Scattering Study of Glasses of Hard Colloidal Spheres. *Phys. Rev. E* **1993**, *47*, 248–261.

(78) Kob, W.; Donati, C.; Plimpton, S. J.; Poole, P. H.; Glotzer, S. C. Dynamical Heterogeneities in a Supercooled Lennard-Jones Liquid. *Phys. Rev. Lett.* **1997**, *79*, 2827–2830.

(79) Roberts, R. C.; Poling-Skutvik, R.; Palmer, J. C.; Conrad, J. C. Tracer Transport Probes Relaxation and Structure of Attractive and Repulsive Glassy Liquids. *The Journal of Physical Chemistry Letters* **2018**, *9*, 3008–3013.

(80) Roberts, R. C.; Poling-Skutvik, R.; Conrad, J. C.; Palmer, J. C. Tracer transport in attractive and repulsive supercooled liquids and glasses. *The Journal of Chemical Physics* **2019**, *151*, 194501.

(81) Sprakel, J.; van der Gucht, J.; Cohen Stuart, M. A.; Besseling, N. A. M. Rouse dynamics of colloids bound to polymer networks. *Phys. Rev. Lett.* **2007**, *99*, 208301.

(82) Rudnick, J.; Gaspari, G. The Shapes of Random Walks. *Science* **1987**, *237*, 384–389.

(83) Flory, P. J. *Statistical mechanics of chain molecules*; Oxford University Press, New York, 1988.

(84) Rubinstein, M.; Colby, R. H. *Polymer Physics*; Oxford University Press: New York, 2003.

(85) Bernabei, M.; Bačová, P.; Moreno, A. J.; Narros, A.; Likos, C. N. Fluids of semiflexible ring polymers: effective potentials and clustering. *Soft Matter* **2013**, *9*, 1287–1300.

(86) Slimani, M. Z.; Bačová, P.; Bernabei, M.; Narros, A.; Likos, C. N.; Moreno, A. J. Cluster Glasses of Semiflexible Ring Polymers. *ACS Macro Lett.* **2014**, *3*, 611–616.

(87) Poier, P.; Bačová, P.; Moreno, A. J.; Likos, C. N.; Blaak, R. Anisotropic effective interactions and stack formation in mixtures of semiflexible ring polymers. *Soft Matter* **2016**, *12*, 4805–4820.

(88) Staňo, R.; Likos, C. N.; Smrek, J. To thread or not to thread? Effective potentials and threading interactions between asymmetric ring polymers. *Soft Matter* **2023**, *19*, 17–30.

(89) Humphrey, W.; Dalke, A.; Schulten, K. VMD: Visual molecular dynamics. *Journal of Molecular Graphics* **1996**, *14*, 33–38.

TOC Graphic